

## Supplementary Information

### Oxygen Tracer Diffusion in Amorphous Hafnia Films for Resistive Memory

Dongjae Shin<sup>1</sup>, Anton V. Ievlev<sup>2</sup>, Karsten Beckmann<sup>3,4</sup>, Jingxian Li<sup>1</sup>, Pengyu Ren<sup>1</sup>,

Nathaniel Cady<sup>3</sup>, Yiyang Li<sup>1</sup>

<sup>1</sup> Materials Science and Engineering, University of Michigan, Ann Arbor, MI, USA

<sup>2</sup> Center for Nanophase Materials Science, Oak Ridge National Laboratory, Oak Ridge, TN, USA

<sup>3</sup> College of Nanotechnology, Science and Engineering, University at Albany, Albany, NY, USA

<sup>4</sup> NY CREATES, Albany, NY, USA

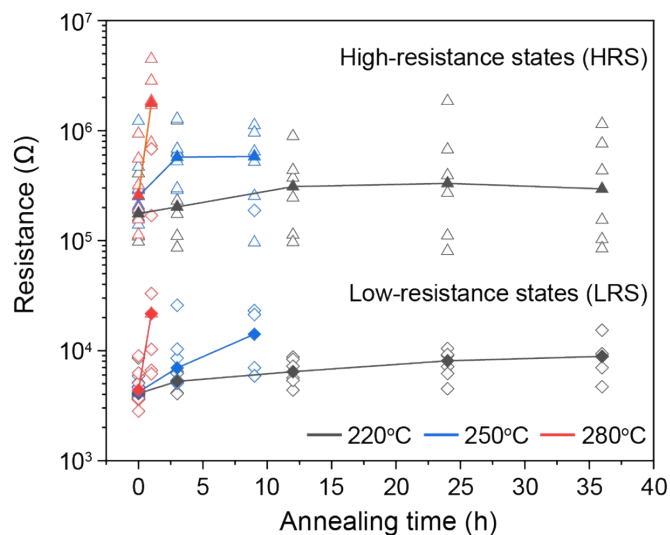


**Figure S1.** Evolution of resistance state of resistive memory devices after annealing at different temperatures. Our results show that the low-resistance state fails into the high-resistance state, suggesting filament dissolution. Each hollow marker shows one device, while the solid marker denotes the median value of six devices.

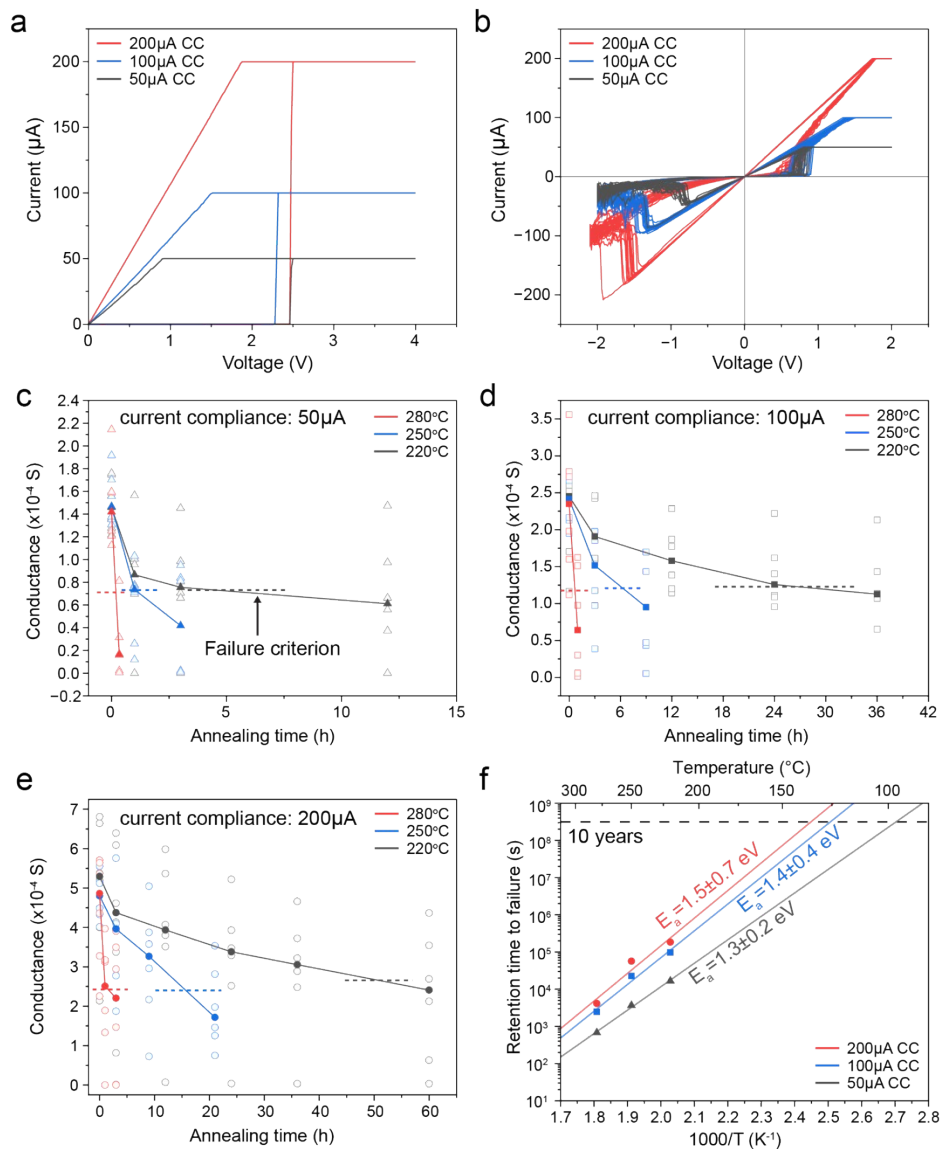


**Figure S2.** Effects of current compliance (CC) on retention: 50 $\mu$ A (black), 100 $\mu$ A (blue), and 200 $\mu$ A (red). **a** current-voltage profiles of the forming process. **b** 20 cycles of DC switching with different current compliances. **c-e** Evolution of the device conductance upon annealing at different temperatures with different current compliance. The empty symbols are conductance values from the 6 devices at each annealing time and temperature (280 $^{\circ}$ C red, 250 $^{\circ}$ C blue, and 220 $^{\circ}$ C black), while the solid symbols represent medians calculated from the six conductance values at each annealing time and temperature. The dashed line indicates failure criteria defined as half the conductance value of the initial median. **f** Arrhenius plots of retention times to failure at different current compliance (200 $\mu$ A red, 100 $\mu$ A blue, and 50 $\mu$ A black). The activation energy of retention time is  $1.5 \pm 0.7$  eV at 200  $\mu$ A current compliance (CC),  $1.4 \pm 0.4$  eV at 100  $\mu$ A CC, and  $1.3 \pm 0.2$  eV at 50 $\mu$ A CC. The 100 $\mu$ A current compliance is the same data as presented in Figure 1d and e. Due to the larger current compliance, the tungsten series resistor in the 200 $\mu$ A experiment is 7 k $\Omega$ , as opposed to 10 k $\Omega$  in all other experiments.

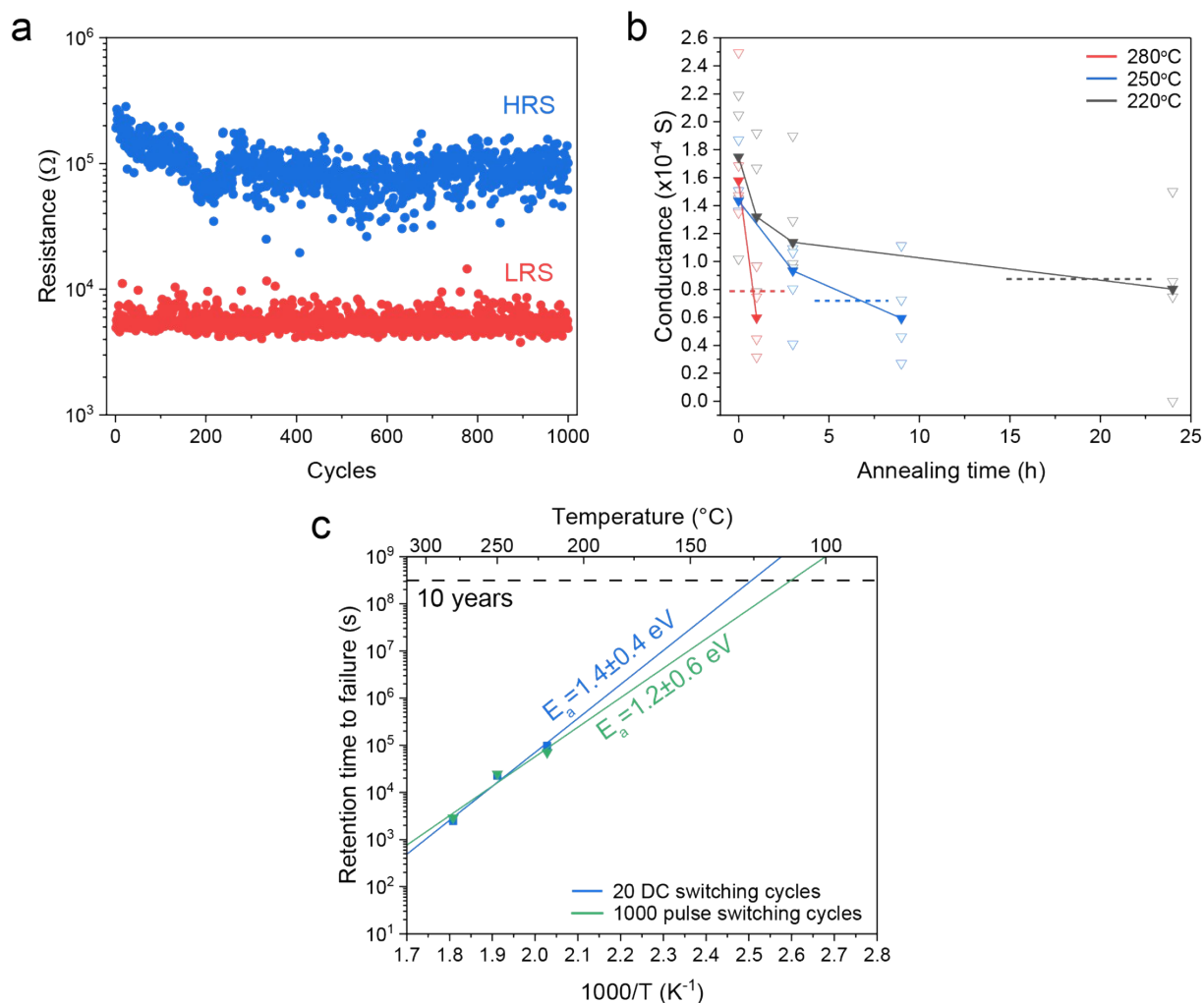


**Figure S3.** Comparison of retention after 1000 pulse switching **a** Typical resistance variation during pulsed switching over 1000 cycles. After DC forming, each cycle composed of following steps: RESET -3V (20 $\mu$ s), READ 0.15 V (20 $\mu$ s), SET 2V (20 $\mu$ s), READ 0.15V (20 $\mu$ s). The current compliance (CC) was set to 10 $\mu$ A. **b** Retention tests after 1000 switching cycles. The empty triangles are conductance values from the 4 devices at each annealing time and temperature (280 $^{\circ}$ C red, 250 $^{\circ}$ C blue, and 220 $^{\circ}$ C black), while the solid triangles represent medians calculated from the four conductance values at each annealing time and temperature. The dashed line indicates failure criteria defined as half the conductance value of the initial median. **c** Arrhenius plots of retention times to failure of 1000 pulse switched devices (green). The activation energy of retention time is  $1.2 \pm 0.6$  eV whereas the activation energy with 20 DC switched devices (100  $\mu$ A CC) from Figure 1e is  $1.4 \pm 0.4$  eV (blue).

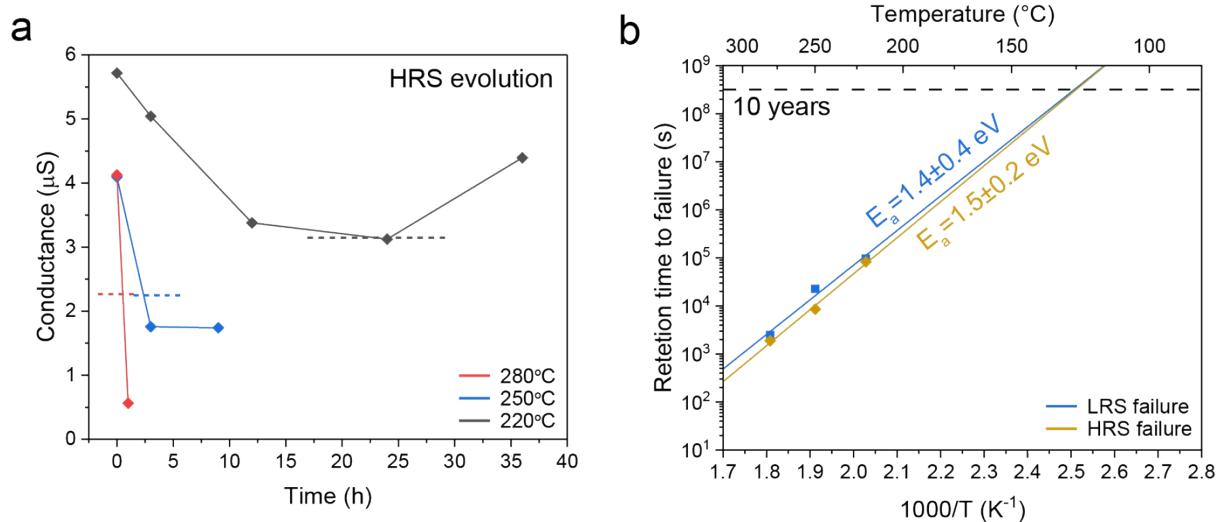


**Figure S4.** Evolution of the HRS conductance at different temperatures. **a** The HRS device conductance upon annealing at different temperatures after 20 cycles DC switching under  $100\mu\text{A}$  current compliance. The solid diamonds represent medians calculated from the six devices' conductance values from Figure S1 at different temperature ( $280^\circ\text{C}$  red,  $250^\circ\text{C}$  blue, and  $220^\circ\text{C}$  black). The dashed line indicates retention criteria defined as 45% decrement from the initial median. **b** Arrhenius plots of retention times of LRS (blue, from Fig. 1e) and HRS (gold) show very similar retention times. Activation energy of HRS failure is  $1.5 \pm 0.2$  eV (gold) whereas the activation energy of the LRS failure from Figure 1e is  $1.4 \pm 0.4$  eV (blue). All results used  $100\mu\text{A}$  current compliance.

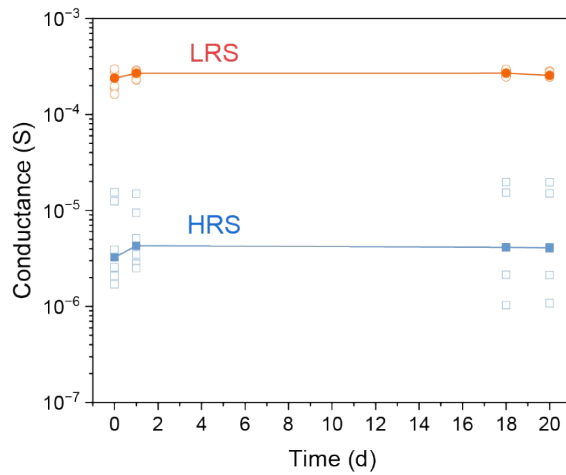


**Figure S5.** Retention data at room temperature. Each device underwent 20 cycles of DC switching with  $100\mu\text{A}$  current compliance. After 20 cycles of switching, 6 devices switched to LRS, while the other 6 devices switched to HRS. The empty symbols represent the data from the 6 devices in LRS (shown in orange) and HRS (shown in blue), while the solid symbols represent the medians of the 6 devices from each state. Over the course of 20 days, none of the devices showed significant changes in the conductance.

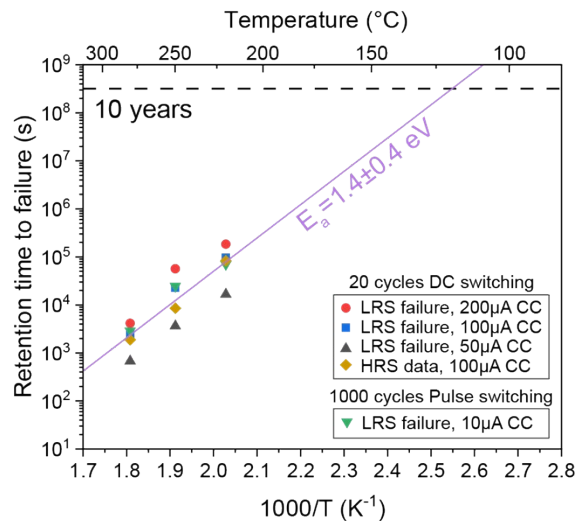


**Figure S6.** Combined retention results from the different switching conditions shown in Fig. S2-4. When all data is combined, the activation energy is  $1.4\pm 0.4$  eV, identical to the one originally calculated in Fig. 1e based on LRS failure with  $100\mu\text{A}$  compliance.

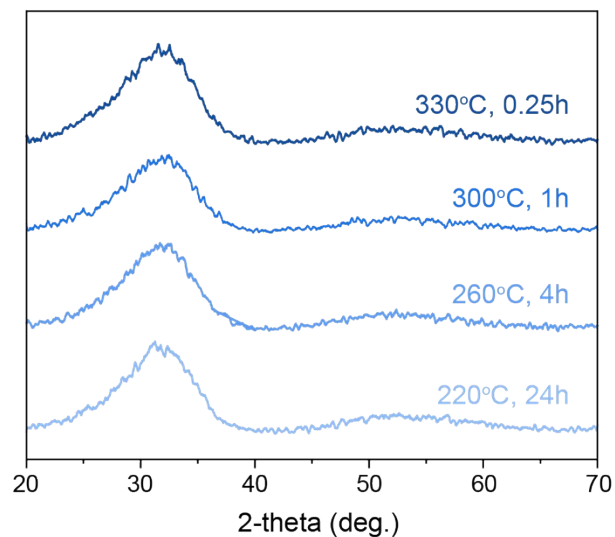


**Figure S7.** X-ray diffraction results of tri-layer samples consisting of sputtered HfO<sub>2</sub> samples. These results show that the films remain amorphous even after the annealing conditions for the isotope tracer diffusion experiments in Fig. 2.

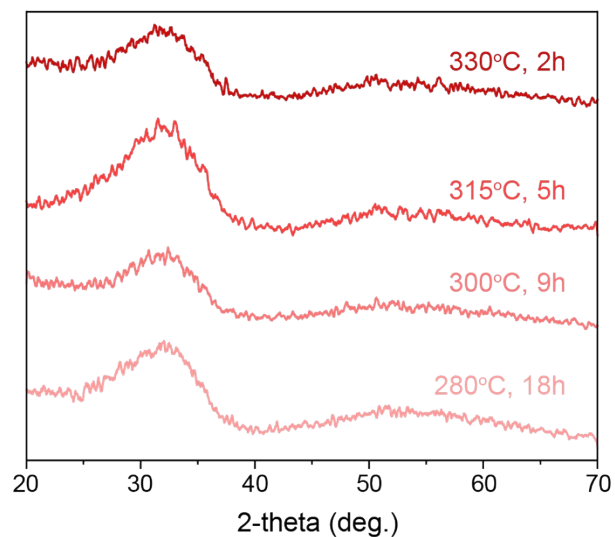


**Figure S8.** X-ray diffraction results of bi-layer samples consisting of a sputtered <sup>18</sup>O-enriched HfO<sub>2</sub> layer above a natural abundance ALD HfO<sub>2</sub> layer. These results also show that the films remain amorphous after the annealing conditions of Fig. 3.

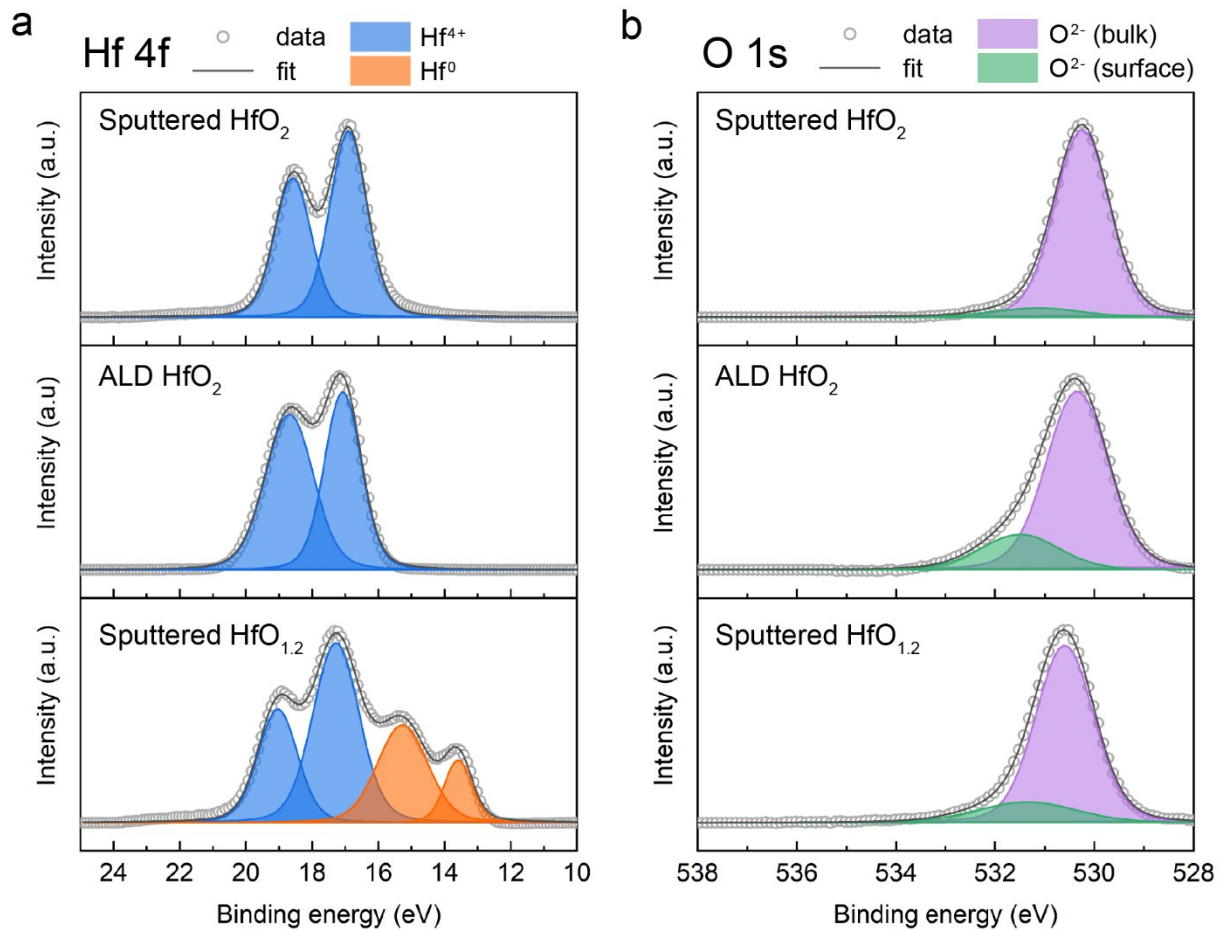


**Figure S9.** X-ray photoelectron spectroscopy (XPS) results of three different types of films: sputtered HfO<sub>2</sub> (top), ALD HfO<sub>2</sub> (middle), sputtered HfO<sub>1.2</sub> (bottom). **a** Hf 4f spectra. **b** O 1s spectra. X-ray photoelectron spectroscopy results show that sputtered HfO<sub>2</sub> and ALD HfO<sub>2</sub> are chemically identical, whereas sputtered HfO<sub>1.2</sub> shows increased metallic Hf due to substoichiometry of the film. This sputtered HfO<sub>1.2</sub> film contained 1.5% O<sub>2</sub>, 98.5% Ar in the sputter gas, as opposed to 10% O<sub>2</sub>, 90% Ar in the sputtered HfO<sub>2</sub> samples.

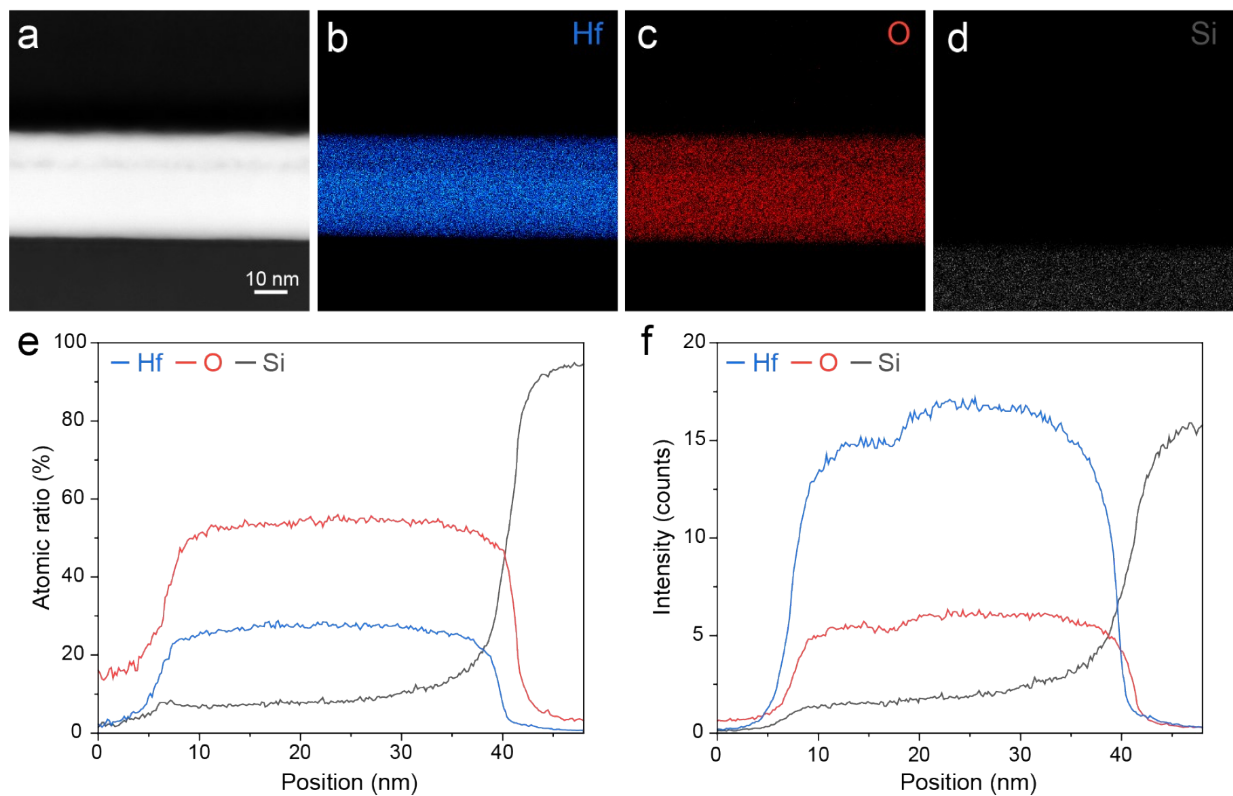


**Figure S10.** Scanning transmission electron microscopy (STEM) of the films. **a** STEM-HAADF image of the bi-layer sample comprising of an  $^{18}\text{O}$ -enriched sputtered  $\text{HfO}_2$  layer above a natural-abundance ALD  $\text{HfO}_2$  layer. **(b-d)** STEM-EDS mapping of Hf, O, and Si. The bottom ALD layer shows greater Hf and O intensity than the top sputtered layer. **(e)** Line scan of the bi-layer film stack shows that the ALD and sputtered layer have the same Hf:O ratio of 1:2. **(f)** STEM-EDS shows higher absolute Hf and O intensity in the ALD layer compared to the sputtered layer.

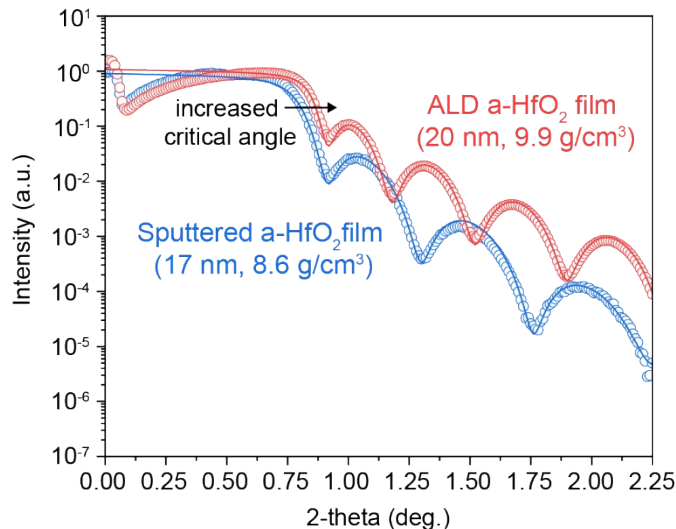


**Figure S11.** X-ray Reflectivity (XRR) measurements of a sputtered a-HfO<sub>2</sub> (blue) and ALD a-HfO<sub>2</sub> (red) show much higher density in the ALD compared to the sputtered film. Empty circles are measured data and solid lines are simulated results. Critical angles are proportional to the densities of films.<sup>1</sup>

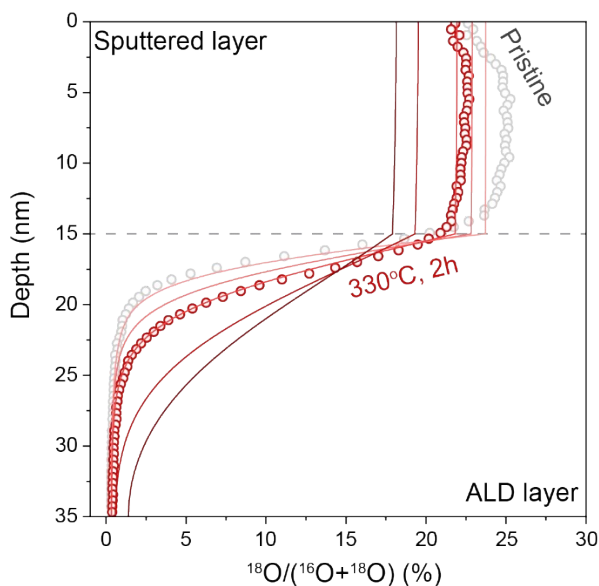


**Figure S12.** To identify the oxygen tracer diffusion in the ALD film, we simulate the evolution of the unannealed Pristine state (gray circles) using Fick's Laws of Diffusion with oxygen tracer diffusion values. We then compute the coefficient of determination ( $R^2$ ) between the experimental data after annealing (red circles) and the simulations (red lines). In this graph, we simulated oxygen tracer diffusion with diffusion values ( $D$ ) of  $1 \times 10^{-4}$  (light pink),  $4 \times 10^{-4}$ ,  $8.8 \times 10^{-4}$ ,  $3 \times 10^{-3}$ ,  $5 \times 10^{-3}$  nm<sup>2</sup>/s (dark red), which yielded  $R^2$  values of 0.951, 0.986, 0.998, 0.933, 0.850, respectively. We pick the oxygen tracer diffusivity that yields the largest  $R^2$  to be the experimentally measured tracer diffusion.

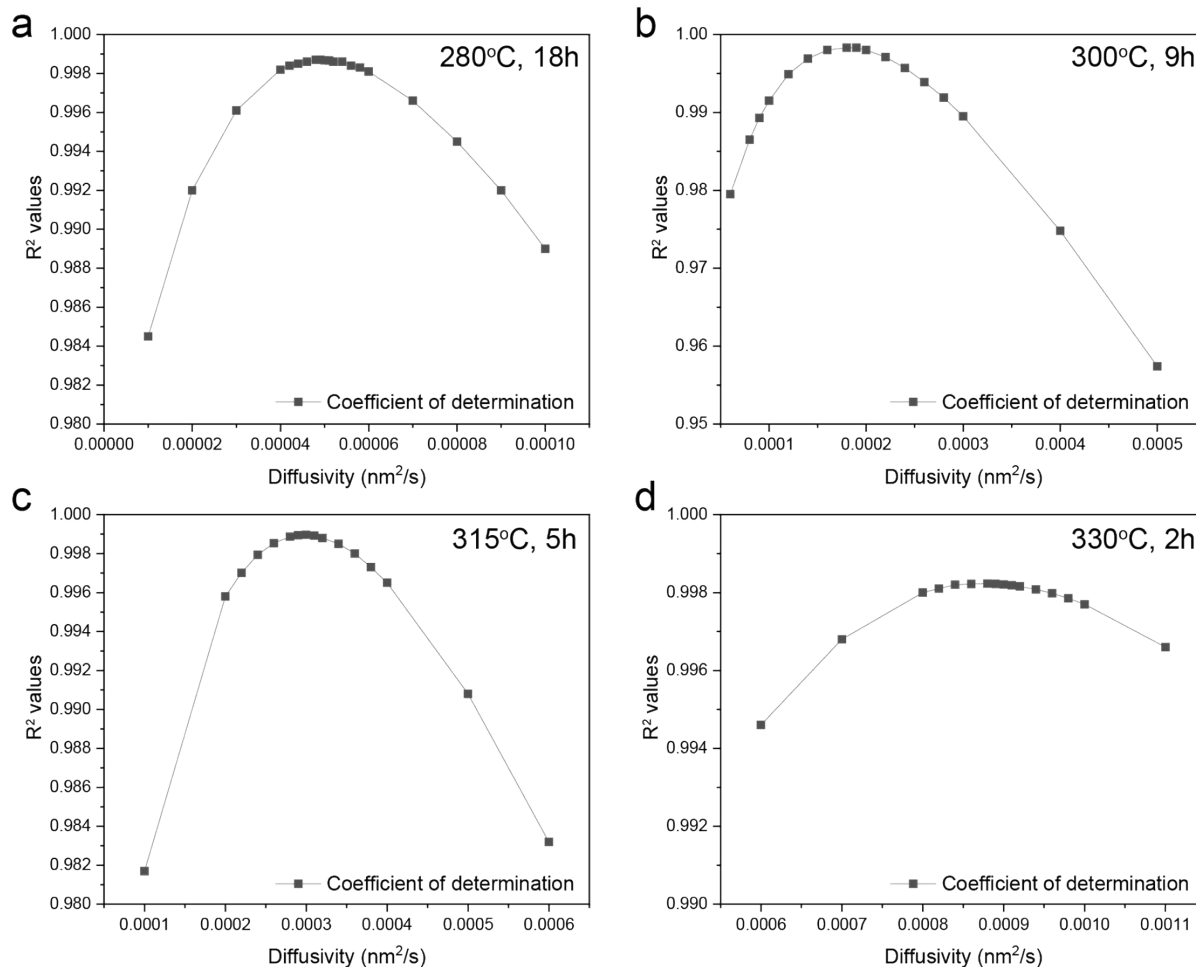


**Figure S13.** Computing the oxygen diffusivity of the ALD films. We numerically simulate the tracer composition using Fick’s Laws of Diffusion and by using the “Pristine” film as the initial condition in the simulation (Fig. S12). We then compute the coefficient of determination ( $R^2$ ) between the experimentally-measured tracer diffusion profile and the simulated results from different simulated values of oxygen diffusivity in the ALD film (x-axis). One example is shown in Fig. S12. We pick the oxygen diffusivity with the highest  $R^2$  value as our estimate for the oxygen tracer diffusion in the ALD film.

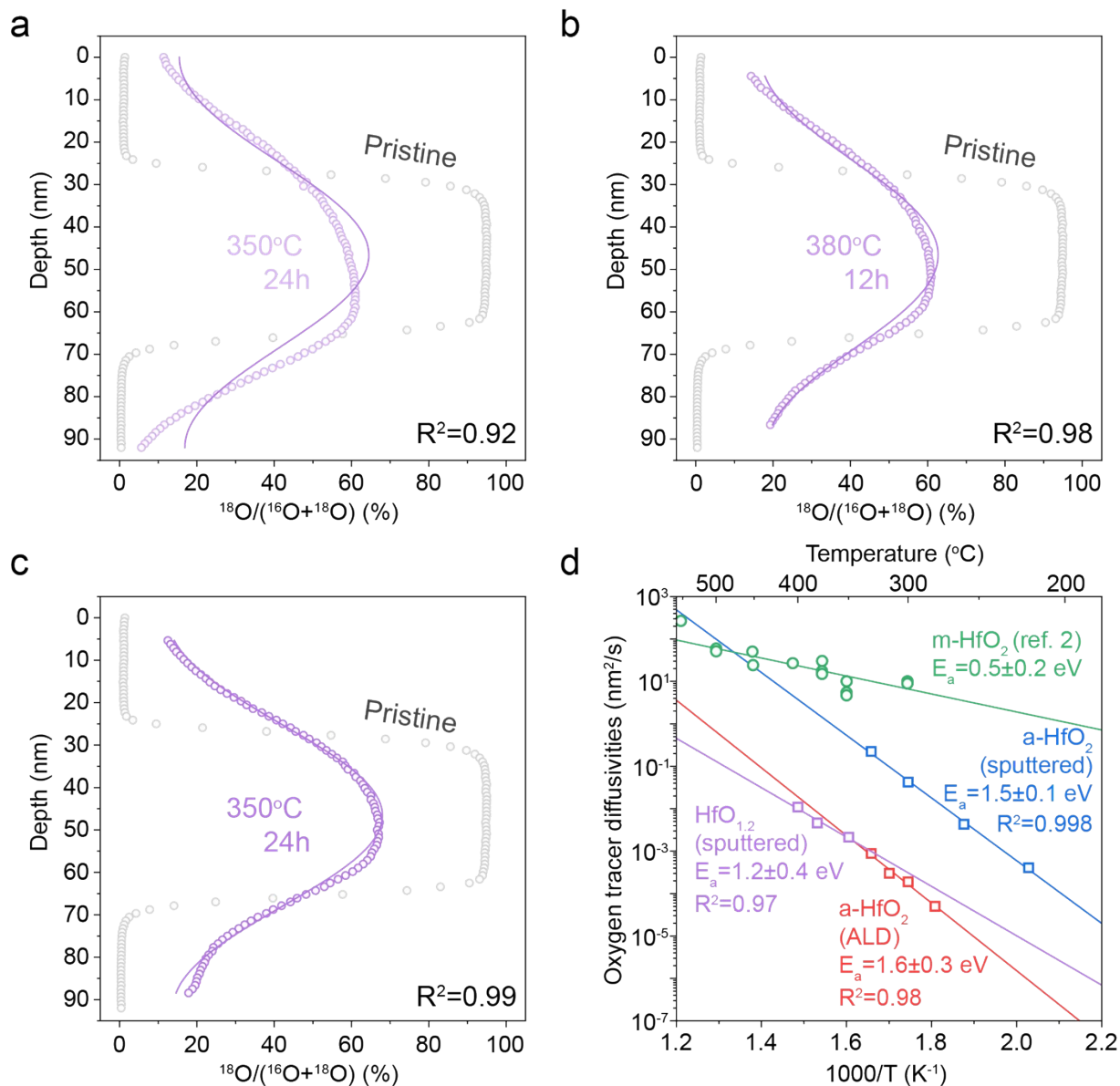


**Figure S14.** Oxygen tracer diffusion measurements for sub-stoichiometric sputtered  $\text{HfO}_{1.2}$ . This film used 1.5%  $\text{O}_2$ , 98.5% Ar in the sputter gas, as opposed to 10%  $\text{O}_2$  for the  $\text{HfO}_2$  samples. **a,b,c** ToF-SIMS depth profiling results of annealed samples (purple empty circles) and pristine sample (grey empty circles). The  $^{18}\text{O}$  middle film uses a pure  $^{18}\text{O}_2$  source for oxygen gas. Purple lines show fitted depth profiles with coefficient of determination values ( $R^2$ ). **d** The Arrhenius temperature plots of the measured oxygen diffusion in different types of  $\text{HfO}_2$  (monoclinic  $\text{HfO}_2$ , amorphous sputtered  $\text{HfO}_2$ , amorphous ALD  $\text{HfO}_2$ , and sub-stoichiometric sputtered  $\text{HfO}_{1.2}$ ). The activation energy of oxygen tracer diffusivities for sub-stoichiometric sputtered  $\text{HfO}_{1.2}$  is  $1.2 \pm 0.4$  eV which is similar value to that of amorphous sputtered  $\text{HfO}_2$  and amorphous ALD  $\text{HfO}_2$ .

Reference (DOI)	Device Configuration	Activation energy (eV)	Switching Method
[16] Azzaz et al. (10.1109/IMW.2016.7495268)	Ti/HfO <sub>2</sub> /TiN	1.09	DC sweep 100μA current compliance (CC)
[17] Chen et al. (10.1109/IEDM.2013.6724598)	Hf/HfO <sub>2</sub> /TiN	1.49	Pulse 40μA CC
[18] Chen et al. (10.1109/TED.2013.2241064)	Ti/HfO <sub>2</sub> /TiN	1.14	Pulse 10μA CC
	Ta/HfO <sub>2</sub> /TiN	1.52	
	Ti/HfO <sub>2</sub> /TiN	1.16	Pulse 100μA CC
	Ta/HfO <sub>2</sub> /TiN	1.33	
[19] Chen et al. (10.1109/IEDM.2012.6479079)	Hf/HfO <sub>2</sub> /TiN	1.51	Pulse 10μA CC
		1.25	Pulse 100μA CC
[20] Traore et al. (10.1109/TED.2015.2490545)	Ti/HfO <sub>2</sub> /TiN	1.49	DC sweep 100μA current compliance (CC)
[21] Zhao et al. (10.1109/IEDM.2017.8268522)	TEL/Al:HfO <sub>x</sub> /TiN (TEL: thermal enhanced layer)	1.36	Pulse

**Table S1.** Summary of retention measurements with device configurations and activation energies.

Device number	Retention time to failure (s) at 220°C	Device number	Retention time to failure (s) at 250°C	Device number	Retention time to failure (s) at 280°C
1	40000	1	7000	1	2000
2	- (over 36 hours)	2	- (over 9 hours)	2	3200
3	110000	3	11000	3	- (over 1 hour)
4	- (over 36 hours)	4	- (over 9 hours)	4	- (over 1 hour)
5	41000	5	8600	5	1200
6	66000	6	- (over 9 hours)	6	2500
Median	<b>97000</b>		<b>23000</b>		<b>2500</b>

**Table S2.** Summary of retention time to failure. The devices are considered to have failed when the resistance doubles from its initial SET value. The measurements were conducted until at least half of the devices failed.

### Supplementary Reference

- 1 C. Lee, W. Choi, M. Kwak, S. Kim and H. Hwang, *Applied Physics Letters*, 2021, **119**, 103503.
- 2 M. P. Mueller and R. A. De Souza, *Appl. Phys. Lett.*, 2018, **112**, 051908.